DAMAGE TOLERANCE AND IMPACT RESISTANCE OF COMPOSITE SCARF JOINTS

Alex B. Harman* and Chun H. Wang*
***Defence Science and Technology Organisation (DSTO).**

Keywords: *damage tolerance, scarf joints, flush repair, composite*

Abstract

The damage tolerance and impact resistance of scarf joints was investigated using experimental and computational (finite element) techniques. It was shown that the presence of the scarf joint reduces the damage tolerance of the parent structure through the introduction of a tapered tip that is both critical to the overall repair strength and also vulnerable to delamination induced by low velocity impact events such as accidental tool drop. The presence of a doubler was shown to improve the damage tolerance slightly at high impact energy levels. A simple analysis method is proposed to enable incorporation of damage tolerance in designing scarf repairs to composite aircraft structures.

1 Introduction

The damage tolerance and impact resistance of scarf joints, which are representative of narrow strips of scarf repairs, with and without an external doubler, was investigated. The results showed that damage to the composite adherends in the scarf joint region, with or without external doublers, resulted in significantly lower adherend strengths than equivalent laminates containing the same level of damage. Based on the experimental observations, the major damage mechanisms following low velocity impact in scarf joints and laminates without repair have been identified. These results demonstrated that it is important to incorporate damage tolerance in the design of scarf repairs over and above the normal static strength considerations.

Flush repairs to military aircraft are expected to become more prevalent as more thick-skin composite structures are used, particularly on the surface of the fuselage, wings and other control surfaces. Flush repairs, whilst difficult to perform, provide a more aerodynamic finish that is also more structurally efficient than standard overlap repairs. However, current scarf repair design methodology does not explicitly consider damage tolerance requirements. It is not clear whether scarf repairs can tolerate the same level of damage as the parent composite laminates.

Representative specimens of base composite laminates and composite scarf joints, with and without external doublers, were tested under compression to determine the compression-strength after impact of the parent structure and the scarf repairs (with and without an external doubler). The effects of impact energy level and location of impact relative to the scarf joint were assessed.

Two simplified analyses were conducted to assist with the interpretation of the experimental test data. The first involved the assumption that the damaged specimens exhibited predominantly brittle behaviour and the second assumed that the behaviour of the specimen was ductile-like (progressive damage in the form of matrix cracking) [1]. If the laminate is assumed to be brittle, provided the stiffness of the damaged region is known, the stress concentration factor around the edge of the approximately circular damaged region can be determined analytically. If ductile behaviour is assumed, the stress concentration near the edge is lessened, resulting in a near constant ligament stress/strain through the net section outside of the damaged region. With these assumptions, the strain in the critical parts of the ligament within the plies and adhesive was determined using linear FEM.

2 Test Methodology

Of particular interest in this test program was to determine the compression after impact (CAI) strength of an un-stiffened parent laminate with and without the presence of a scarf repair. To this end, additional tests were carried out to support the interpretation of the results, such as testing of specimens to failure in tension and strain surveys to measure the modulus and amount of load-bypass with varying specimen width in tension and compression. However, only the CAI results are considered in this paper, with reference made to a published doctorate thesis [2] by the first author that provides a more detailed description of these test programs and the results. Two types of repair were considered: (i) a flush scarf repair and (ii) a scarf repair with a two-ply doubler. The test matrix is shown in Table 1 below. Only ambient temperature tests were conducted in this program.

Table 1 Test matrix

Test description	Number of specimens
CAI of parent specimens (Impact={0,9.5,11.0,13.2, 14.6,16.8,18.4}J)*	10**
CAI of scarf joint specimens, impacted 8mm from the tip (Impact=={0,9.5,11.0,13.2, 14.6,16.8,18.4}J)*	13**
CAI of scarf with doubler joint specimens impacted 8mm from the tip (Impact=={0,10.8,12.7,15.2, 17.5,18.5,21.4}J)***	12**

* BVID for the parent and scarf specimens was determined to be approximately 18.4 Joules.
** Including two undamaged baseline specimens.
*** BVID for the scarf with doubler specimen was determined to be approximately 21.4 Joules.

2.1 Specimen description

The parent laminate consisted of 21-ply Cytec IM7/977-3 prepregs, with layup [±45, 90, 0_3, -45, 0_2, +45, 90, +45, 0_2, -45, 0_3,90, ±45]. The ply percentage of this laminate is [47/38/15]%, representative of an F/A-18 control surface skin. The adhesive chosen for the scarf and doubler joints was Cytec FM73, as considerable Krieger thick adherend test data are available for this adhesive system, which has been used extensively in bonded repair of aircraft structures.

The CAI specimen geometry conformed to the recommendations of the SACMA 2R-94 [3] test method, whereby the specimen length was 150mm and the specimen width was 100mm. During impacting and strength testing, the specimen was clamped on the edges. Each of the scarf joints was manufactured with a CNC-router to give an accurate scarf angle of 5°. A side view of each specimen is shown in Figure 1. The CAI test procedure is described in Section 2.5.

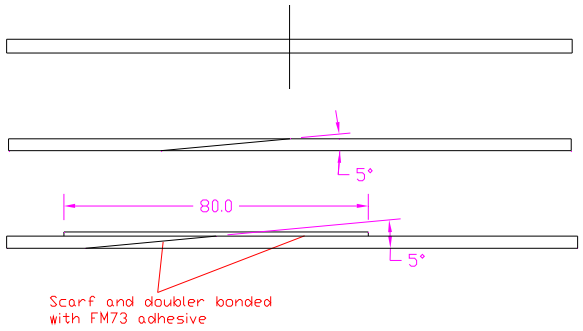

Figure 1 CAI specimen side view

2.2 Impacting procedure and data acquisition

The low velocity impacting rig consisted of a drop weight of approximately 1.5kg running on a vertical rail and a support base to which specimens were clamped to prevent movement during impact. The drop weight had a spherical tup shaped to represent common tools.

Tup diameters of 25mm and 12mm were tested on dummy specimens, with the 12mm tup selected for use during the main CAI program. This decision was somewhat arbitrary with typical certification plans having to account for various tup sizes, but it was considered that the 21 ply laminate used herein was more likely to be on secondary structure, which may not need to consider the damage caused by a 25mm diameter tup.

A force transducer was attached to the tup to measure the force-time history during the impact event. The absorbed energy during

impact is essentially the area below the force-time histogram. Results from the impact testing are provided in Section 4.2.

2.3 Non-Destructive Evaluation (NDE)

The damage within the laminate and joint following low velocity impact can be considerable with modes ranging from delamination between the plies, matrix cracking within the plies and fibre breakage. Typically, the size of the internal damage is much greater than that seen visibly in the form of a dent or a penetration hole. In fact, when a damage is clearly visible with the naked eye, the internal damage may be considerable. An ultrasonic probe can be used to detect internal delaminations and matrix cracking by sending a pulse through the laminate which reflects in areas where the damage has caused air gaps. As shown in Figure 2, a C-scan and an A-scan technique were used to effectively map the area of damage around the impact site. Results from the Non Destructive Evaluation (NDE) are provided in Section 4.2.

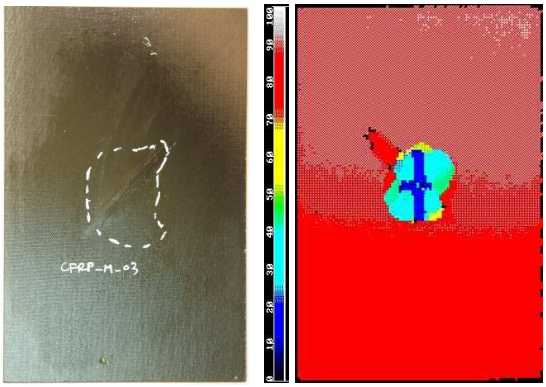

Figure 2 Digitised images using the A-scan (left) and the C-scan (right) technique

2.4 Sectioning

Several of the dummy specimens were sectioned through the impact site to gain more information on the internal damage caused by impact, particularly in the region surrounding the scarf joint.

To obtain optical images of damage, sectioned specimens were first polished with 1200 grit emery paper to make visible the different ply orientations when viewed in ambient conditions and photographed with a macro lens. Next the cut surface was coated with fluoroscene, a fluorescent dye formulated especially to aid NDE. The dye was non-viscous, which allowed it to flow into small areas of damage. The surface was wiped clean with an alcohol based solvent leaving only dye that had been trapped in the damaged regions. The ambient light was removed and an ultraviolet (UV) lamp was used to illuminate the laminate, which caused the damaged regions with the dye to glow. This was photographed also. The two images were morphed into one with an image processing tool, which allowed viewing of the ply orientations and the damage in a single image. The ambient, UV and morphed images of a damaged laminate are shown in Figure 3. Note that the specimen shown was cut along the transverse direction of the laminate. Results from the sectioning are provided in Section 4.2.

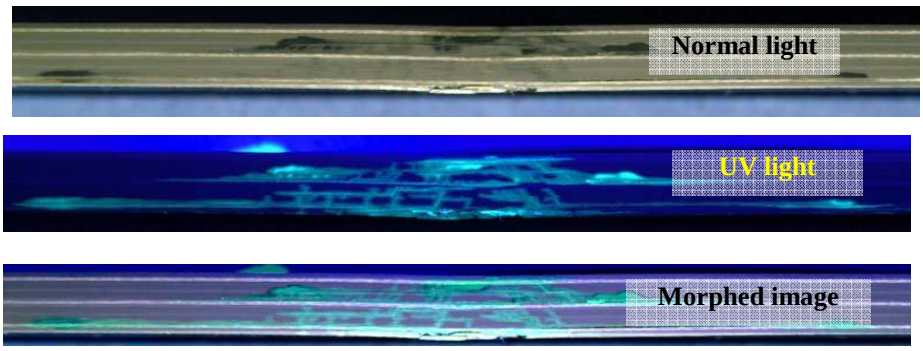

Figure 3 Cross section of a damaged area within a parent adherend specimen

2.5 Test procedure and data acquisition

The CAI test fixture was manufactured as per SACMA 2R-94 method recommendations. The fixture is shown with a specimen installed in Figure 4.

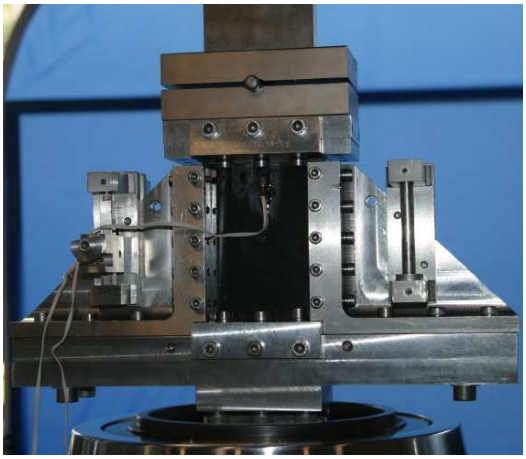

Figure 4 SACMA CAI Test fixture

Each specimen was loaded to failure in compression under displacement control at a rate of 0.5mm/min. The load and crosshead displacement were recorded at 1Hz. Back-to-back strain gauges were installed 25mm from the top, and central width for the majority of specimens, with extensometers used in the same location to measure the strain in the remaining specimens. Sampling was at 1Hz. Results from the CAI test program are provided in Section 4.2.

3 CAI Specimen analyses and FEA methodology

3.1 Analysis methodology

Simplified analyses were performed within this study to aid in the interpretation of the experimental test data. As shown in [2], low velocity impact damage reduces the local modulus, thus causing load redistribution around the damage during uni-axial loading. This is analogous to a uni-axially loaded plate containing a low stiffness inclusion, whereby a stress concentration is introduced at the edge of the damage. As such, damage progression likely to cause final failure is assumed to occur once the stress in the undamaged ligament region reaches a critical level. The damaged region is assumed to be a reduced modulus insert, whereby damage progression is constrained by the “good” material around it.

If the laminate is assumed to be brittle, the stress and strain will concentrate at the edge of the damaged region according to the equation below,

$$\frac{\sigma_{edge}}{\sigma_{applied}} = \frac{3}{1+2E_{insert}/E_{parent}}. \qquad (1)$$

where E_{insert} denotes the modulus of the damaged region.

In the limiting case of the hole, $E_{insert}=0$, therefore $\sigma_{edge}/\sigma_{applied} = 3$. In the present case of impact damage, the modulus of the damaged

zone has been experimentally measured using strain gauges. The results showed that the modulus was around 60% [2] of the parent. This will yield a stress concentration factor of $\sigma_{edge}/\sigma_{applied} = 1.4$. This concentration factor applies to all damage sizes, but the actual failure stress would also depend on the size of damage [4]. This is shown schematically in Figure 5, which showed that damage size has a relatively minor influence.

If the composite laminate is assumed to undergo non-linear deformation (e.g. progressive damage due to matrix cracking) prior to final failure, then the local non-linear deformation of the composite may cause the stress concentration to diminish, thus the stress field becomes approximately uniform across the ligament. Since the ligament width is dependent on the size of damage (d) and the overall specimen width (W), the failure stress predicted using this approach will depend on the d/W ratio for each of the damaged specimens. Therefore, if greater impact energy causes a larger area of damage, the predicted failure will be affected accordingly. The average stress in the ligament region of the specimen is given by

$$\frac{\sigma_{ligament}}{\sigma_{applied}} = \frac{W - E_{insert}/E_{parent}\,(3d - 2W)}{(W - d)(1 + 2\,E_{insert}/E_{parent})}. \qquad (2)$$

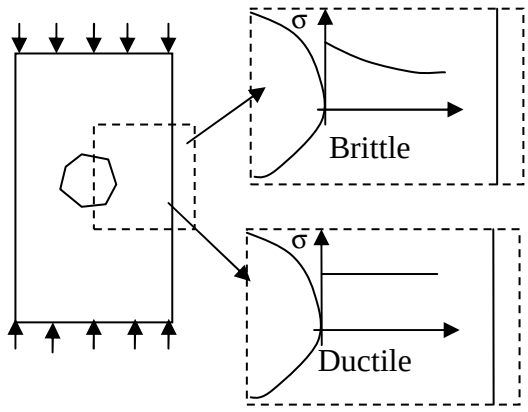

Figure 5 Schematic of residual strength analyses

3.2 FEA of critical elements

Once the local stress field was available using either ductile or brittle assumptions, 2D FEA was performed on sections of the specimen ligament parallel to the load direction to determine the ply and adhesive strains at the failure load for each of the specimens. Also, FEA was able to determine the extent of any strain concentrations that occurred within the scarf joint adherend or adhesive as a result of stacking sequence, particularly near the tip region of the scarf.

The type of mesh used for the parent laminate, scarf and scarf with doubler is shown in Figure 6. The example shown is a section through the scarf joint. The colors represent the different material properties used for the layers, with 0° plies shown in light blue, ±45° plies represented by light purple and dark blue, 90° plies represented by royal blue and the adhesive line represented by dark purple. Six-noded wedge elements have been used with three elements through the thickness of the plies and the adhesive. The model only comprises one element in the width direction, with plane strain assumptions applied. MSC.Nastran was used to perform LEFEM. Since, the failure loads within the specimen did not cause the adhesive to yield at any location along the scarf, non-linear FEA was not required.

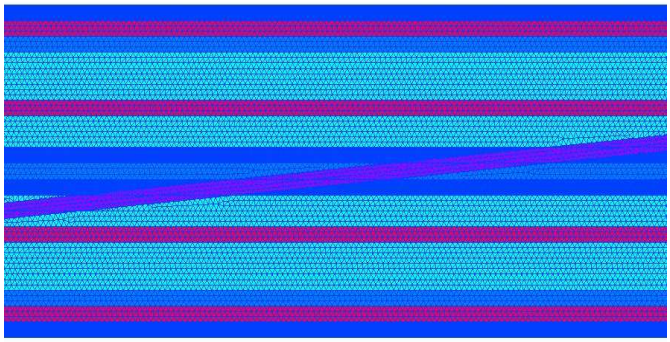

Figure 6 Typical FE mesh used for modeling the laminate and joint

4 Results

4.1 General

The results from the CAI testing, including the impacting, damage assessment

and residual strength test results, as well as FEA results used to determine the ply and adhesive strains in the specimen ligaments at the time of failure are presented in following section.

4.2 Impact test results

A number of dummy and CAI specimens were impacted at varying energy levels to establish the relationship between impact energy and the damage size for each of the specimen types. Impact damage was characterized using pulse-echo C-scanning to determine the damage area within the laminate. The final graph showing the correlations is provided in Figure 7.

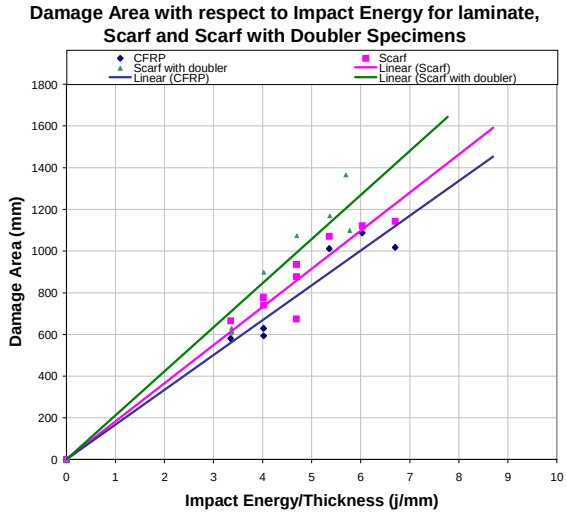

Figure 7 Damage area vs impact energy for each of the specimen types (laminate, scarf and scarf with doubler).

These results show that an approximately linear correlation existed between damage area and impact energy.

The shape of the damage caused in plan view can be seen in the C-scan images provided for each of the specimen types in Figure 8. These results show that the damage at lower energy levels is approximately circular, but as the energy level increases, the damage shape becomes more elongated along the 45° plies, particularly near the back face.

The damage introduced within the internal structure of the laminates could only be determined by destructively sectioning damaged dummy specimens following the impact event. A transverse cut is shown of the laminate specimen in Figure 9. These results show significant delamination progression caused in the central and back surface 45° and 90° plies.

A longitudinal cut through the scarf specimen is shown in Figure 10. These results also show significant delamination caused in each of the 45° and 90° plies. Of particular note is that both tips of the scarf joint are damaged significantly.

The effect of impact location of the type of damage caused within the scarf specimen was also considered. Longitudinal cuts through five specimens impacted with a constant impact energy at various locations ranging from directly over the scarf joint tip, x=0mm to 20mm from the scarf tip (x=20mm), within the joint itself are shown in Figure 11. These results show that the pattern of damage to the scarf joint is strongly dependant on the location of impact relative to the scarf joint tip. It may be that the most severe damage is caused when the impact is at some distance away from the tip, where damage may be caused to both scarf tips.

At one impact location, x=0mm, minimal damage is caused to the tip itself with damage extending to the back face tip. At other impact locations, damage to both tips is clearly seen. It can also be seen that the adhesive line slows the progression of delaminations, with the impact at the midpoint of the scarf (x=15mm) showing the least amount of damage.

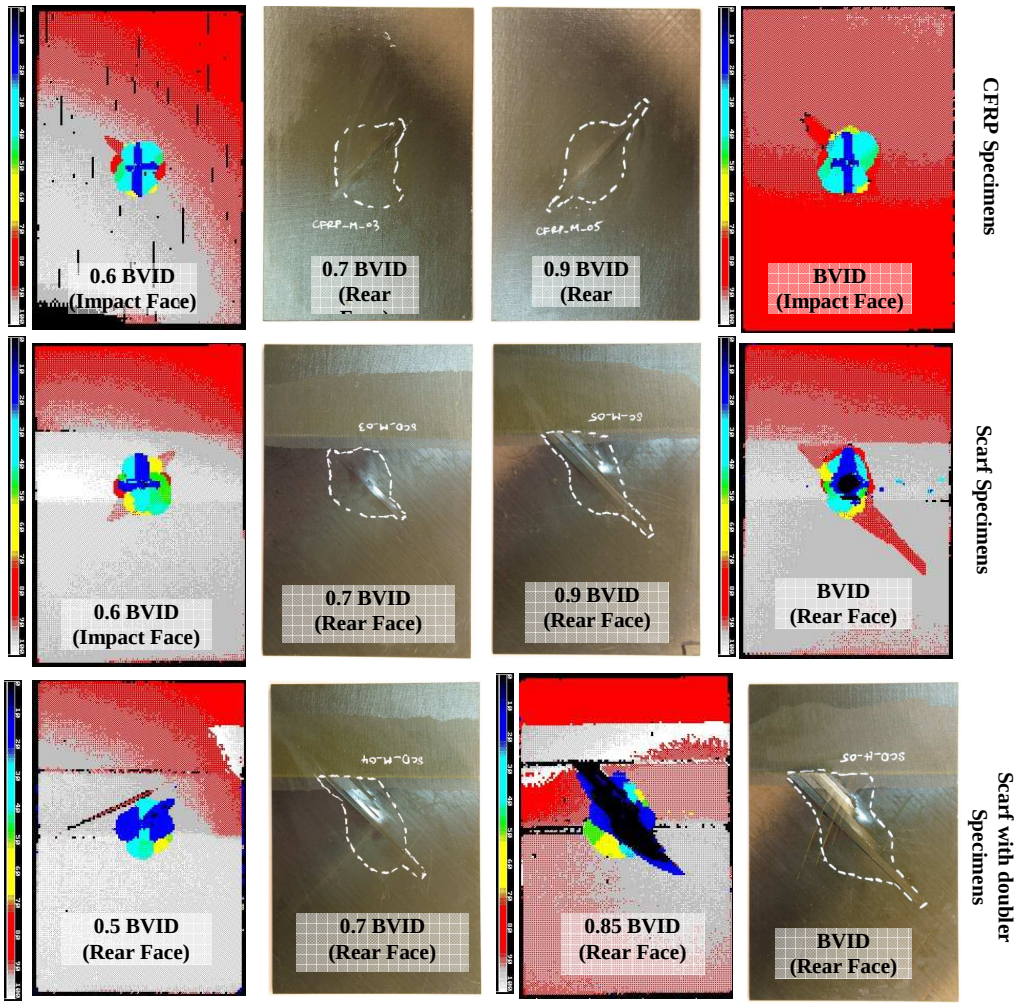

Figure 8 C-scan images for each of the specimen types at energy levels rising from 0.5BVID to BVID.

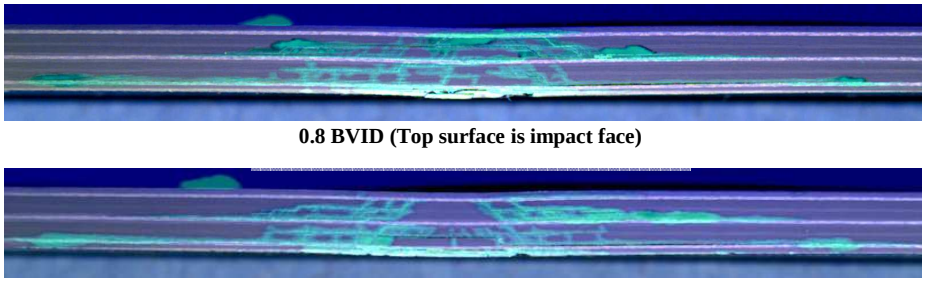

0.8 BVID (Top surface is impact face)

1.1 BVID (Top surface is impact face)

Figure 9 Transverse cut through two laminate specimens impacted with 0.8BVID (top) and 1.1BVID (bottom).

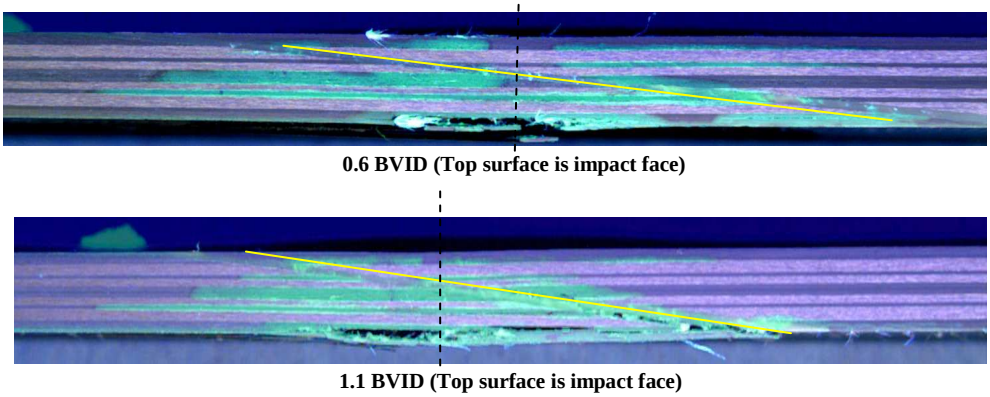

Figure 10 Longitudinal cut through two scarf specimens impacted with 0.8BVID (top) and 1.1BVID (bottom).

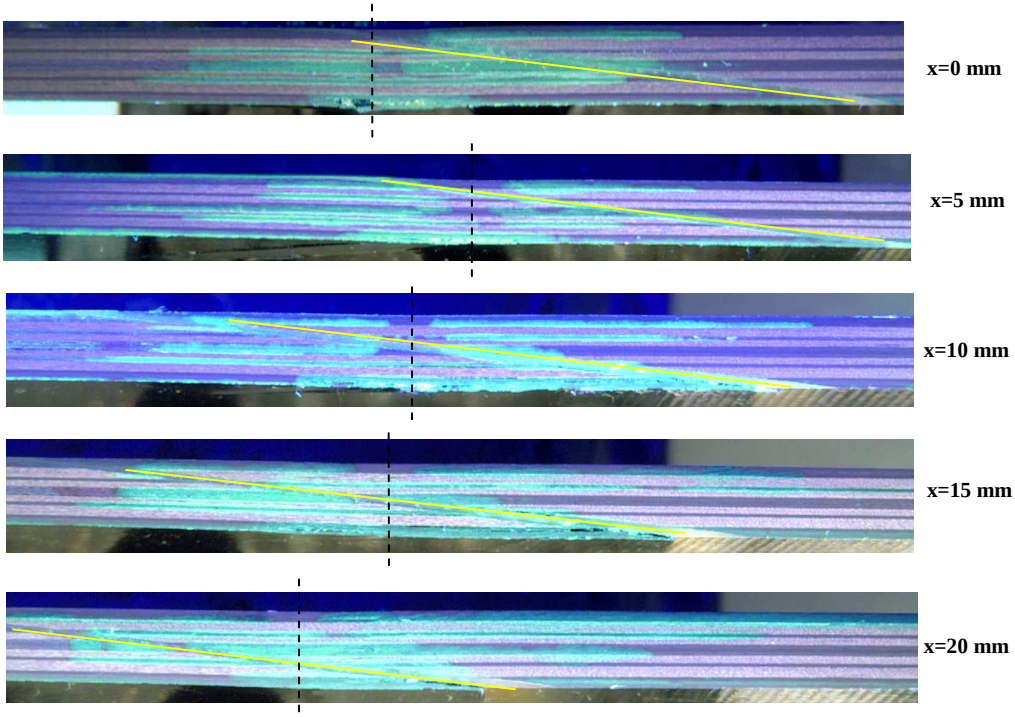

Figure 11 Longitudinal cut through five scarf specimens impacted with 0.6BVID at various distances (x) away from the scarf joint tip.

4.3 CAI Test results

The results from the residual strength testing have been presented in two ways. The first is far field strain at the time of failure with respect to impact damage area (Figure 12), and the second is the calculated average ligament strain (Figure 13) assuming the adherend material to behave in ductile manner with respect to damage area. All results are normalized with the un-notched compression failure strain of the parent laminate which equated to 4300με. This value is expected to be the lower bound for the compression strength of this laminate, as some evidence of buckling was observed in the gap region of the test fixture despite edge and end clamping of the specimen that exceeded the requirements of the test method. These results show a clear reduction in strength with increasing damage area for all specimen types. The results also show that the average ligament strain at failure in the scarf joint specimens is almost consistently 20% lower than the parent

laminate ligament strain for a given damage area. This suggests that the strength differential between the parent laminate and the scarf joint is maintained with increasing damage up until the point where significant scarf damage occurs at the higher than BVID impact energies. This may provide a simplified tool for determining the strength of the damaged scarf joint based on a known undamaged strength and the area of damage that occurs within the scarf joint. These results show that at the lower energy levels the doubler has no effect on the failure strain of the scarfed adherend, but at the high energy levels, the doubler prevents the dramatic reduction in strength observed in the scarf specimens.

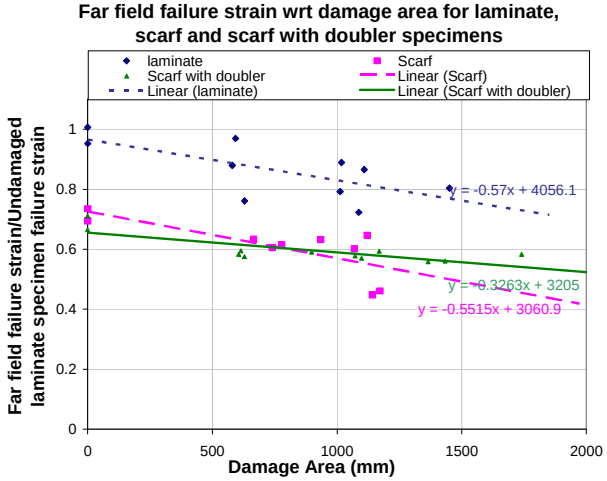

Figure 12 Far field failure strain with respect to impact damage area

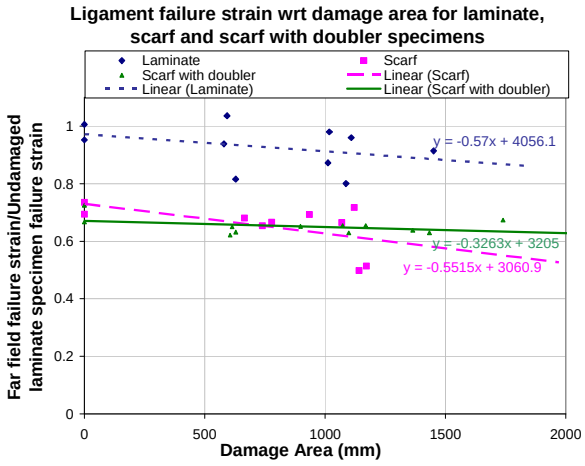

Figure 13 Average ligament strain at failure with respect to impact damage area

4.4 CAI Specimen failure modes

Following failure, the CAI specimens were sectioned through the ligament region to observe the modes of failure. The internal damage at the failure location of the parent laminate specimen is presented in Figure 14. This shows significant delaminations caused near the surface plies of the laminate and evidence of micro-buckling in the 0° ply groups. It is possible that the surface plies delaminated initially, thus destabilizing the laminate and eventually allowing micro-buckling in the 0° ply groups.

The failure of the scarf joint in compression is shown in Figure 15. The failure appears to be predominantly matrix cracking and inter-ply delamination within the adherend. There was no clear indication of the scarf joint adhesive failing within any of the sections across the specimen. Significant delamination can be seen adjacent and through the 45° and 90° layers. There is also evidence of the 45° and 90° plies nearest the impact surface (top surface) buckling locally. The delaminations can also be seen to be halted or redirected by the presence of the scarf bondline, adding further evidence that the adhesive was not overloaded, or had even yielded prior to specimen failure.

The failure of the scarf with doubler joint shown in Figure 16, however shows evidence of failure within the joint adhesive, or at least through the ply matrix close to the adhesive. The buckling of the outer plies observed in the scarf joint failure appears to have been mitigated by the presence of the doubler. However, there is evidence of the plies of the back face delaminating near the scarf tip, extending from the 90° ply adjacent to the 0° group closest to the back face.

Figure 14 Failure location of the parent laminate specimen

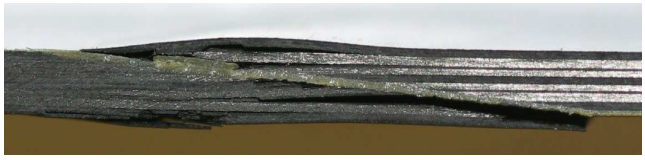

Figure 15 Failure location of the scarf joint specimen

Figure 16 Failure location of the scarf joint with doubler specimen

4.5 LEFEA of the parent laminate and the scarf joint

In this study, FEA was used to understand further the failure mechanisms within the parent laminate and scarf joint specimens. The strains within the adherend plies or in the adhesive at failure depended on whether a brittle or a ductile failure was assumed to occur. As discussed in Section 3.1, if the adherend behaviour is brittle, the ligament stress concentrates near the edge of the damaged region at a level independent of damage size. However, if the adherend behaviour is ductile the ligament stress is uniform and is dependant on the damage size and overall specimen width. Since matrix failure was observed in both the laminate and scarf specimens, of particular interest were regions of first invariant strain, J_1 and Von Mises strain, ε_{vm} concentration in the 45° and 90° plies. It was also of interest to determine if the adhesive in the scarf was close to yielding at any location within the specimens prior to specimen failure.

A plot of the strain through the thickness of the laminate showed that the peaks occurred in the outer three 45° and 90° plies. As such, only the strain distribution in the outer four plies is shown in Figure 17. These results show that the Von Mises strain peaks at the interface between the 45° plies and the J_1 peaks within the 90° ply. This is consistent with observations by Gosse [5] using the Strain Invariant Failure Theory (SIFT).

FEA of the scarf joint showed that a significant strain peak was observed at the interface between the 90° and 0° ply closest to the scarf joint tip. Observations of the scarf joint failure modes confirmed that this may be a site of failure initiation. A plot of the Von Mises and J_1 strain from the 0° to 90° interface (peak) along the path of highest strain is shown in Figure 18. These results show that the strain concentration in the scarf joint adherend far exceeds that in the parent laminate, which would explain premature failure of the specimen, despite it being an adherend failure rather than a cohesive failure through the scarf joint adhesive. As discussed the strain concentration causes the ligament strain to be 40% greater than the applied strain at failure. This equates to an applied ligament strain of 6000με. A plot of the shear strain in the scarf joint adhesive subjected to an applied strain of 6000με is provided in Figure 19. These results show that at this load, the peaks in the adhesive shear strain do not exceed the elastic limit of the adhesive. Therefore, it is unlikely that the adhesive failed prior to overall specimen failure.

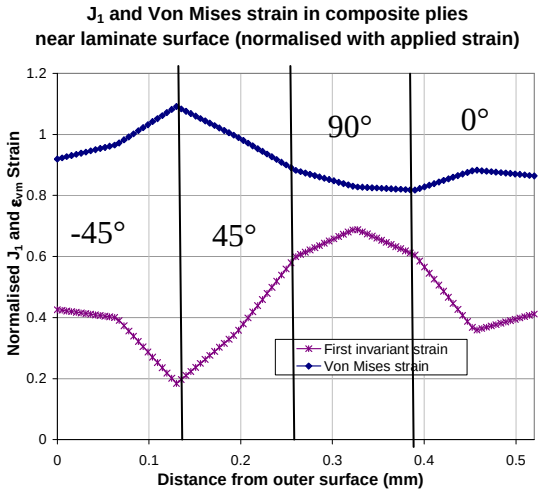

Figure 17 Strain in outer four (-45/45/90/0) plies near the parent laminate surface

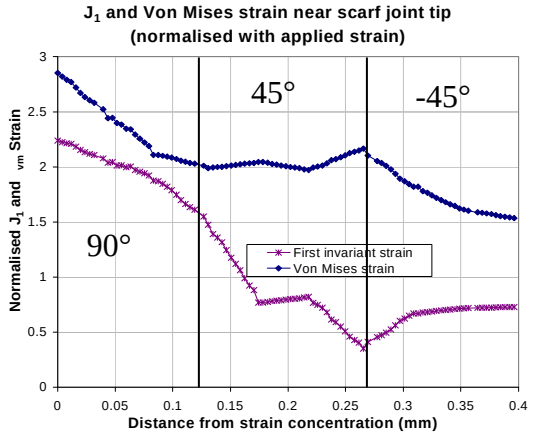

Figure 18 Strain distribution from the peak strain location to the outer surface of the tip.

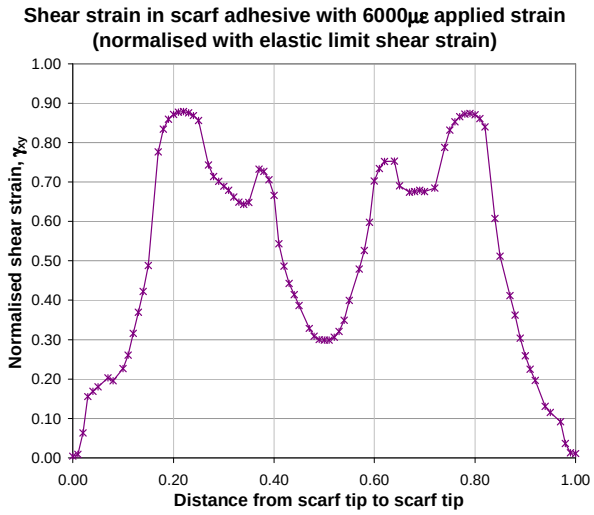

Figure 19 Shear strain distribution at the extreme ligament strain for the scarf joint specimens.

5 Implications for scarf repair design

The design of scarf repairs to composite aircraft structures are assumed in the current design practice to be as damage tolerant and impact resistant as their parent structures. Evidence of the delaminations halting or changing path at the adhesive bondline supported the argument that the addition of a toughened adhesive system such as FM73 improves the impact resistance of the parent structures. However, evidence was also provided that showed that a low velocity impact near the tips of a scarf repair causes delaminations that extend through 45° and 90° plies, typically placed on the surface of the parent structure, and into the tip region of the scarf. This was shown to reduce the strength of the scarf joint in compression, with observations made of the outer plies near the scarf tip buckling both within the damaged region and within the ligament outside the damaged region. Results of finite element analysis also confirmed that a strain concentration can occur within the scarf joint adherend tip region that may cause failure to initiate in the adherend matrix near to the scarf joint tip at much lower strains than the un-notched strength of the parent structure. As such, the presence of a scarf repair may in fact make the structure less tolerant to damage caused by low velocity impact events such as accidental tool drops.

Evidence was also gathered to show that the doubler over the scarf may in fact help to make the repair more damage tolerant at higher impact energies. At impact energies that are close to causing BVID, the scarf joint was shown to dramatically reduce in strength. A damage area limit was reached which resulted in a step reduction in the scarf joint strength. The presence of the doubler was found to raise this limit above the threshold for BVID for these specimens.

Finally, a method for scarf repair design that considers damage tolerance philosophies was developed. It was shown that the damage caused to the scarf joint and parent structure reduces the local modulus within the damaged region. Load is then forced to redistribute around the damage region. Assuming that the damage caused by low velocity impact is effectively constrained within the “good” material surrounding it, failure of the damage area is governed by the failure strain within the structure or ligament surrounding the damage. If the ligament strain is known, undamaged 2D scarf joint and parent laminate strength predictions may apply to determine if the

residual strength of the structure remains above the design limit.

6 Conclusions

The presence of the scarf joint within the parent structure has been shown to reduce the damage tolerance, thus requiring damage tolerance philosophies to be applied in designing repairs to ensure repairs can meet the design requirements.

The presence of a doubler was shown to prevent the large drop off in residual strength of the scarf joint at energies approaching BVID, thus improving damage tolerance of the scarf repair.

A simple design tool is proposed to allow damage tolerance philosophies to be considered within the design of scarf repairs.

7 Acknowledgements

This work contributed to work programs that were funded and supported by the Cooperative Research Centre for Advanced Composite Structures (CRC-ACS) and the Defence Science and Technology Organisation (DSTO).

8 References

1. Eisenmann, J.R. and C.Q. Rousseau, *IBOLT: A composite bolted joint static strength prediction tool*, in *Joining and repair of composite structures*, K.T. Kedward and H. Kim, Editors. 2004, ASTM. p. 161-181.
2. Harman, A., *Optimisation and improvement of scarf repairs to aircraft, PhD. thesis*, in *Faculty of Engineering*. 2007, University of New South Wales: Sydney.
3. Association, S.o.A.C.M., *SACMA Recommended Test Method (SRM 2R-94) for Compression after impact properties of oriented fiber-resin composites*. 1994.
4. Whitney, J.M. and R.J. Nuismer, *Stress fracture criteria for laminated composites containing stress concentrations*. Journal of Composite Materials, 1974. **8**: p. 253-265.
5. Gosse, J.H. and S. Christensen. *Strain invariant failure criteria for polymers in composite materials, AIAA Paper 2001-1184*. in *AIAA/ASME/ASCE/AHS/ASC Structures, Structural Dynamics, and Materials Conference and Exhibit, 42nd*. 2001. Seattle, WA, UNITED STATES.